

Broadband Infrasound Signal of a Collapsing Glacier

Emanuele Marchetti¹, Fabian Walter², Lorenz Meier³

¹Department of Earth Sciences, University of Firenze, Firenze, Italy.

²Laboratory of Hydraulics, Hydrology and Glaciology VAW, ETH Zürich, Switzerland.

³Geopraevent AG, Zürich, Switzerland.

Key Points:

- Glacier collapse is recorded as a broadband infrasound signal.
- Array analysis allows to detect the high ($>1\text{Hz}$) frequency component and derive velocity and trajectory.
- The low ($<1\text{ Hz}$) frequency component is interpreted as air flow around the moving ice mass.

Corresponding author: E. Marchetti, emanuele.marchetti@unifi.it

Abstract

A major ice collapse ($\approx 20,000 \text{ m}^3$) from a hanging glacier on Mount Eiger, Switzerland was recorded by a small aperture array as a broadband (0.1-10 Hz) infrasound signal. Array analysis reveals that the high ($\approx 3 \text{ Hz}$) frequency signal is infrasound produced by the moving ice mass, and its back-azimuth variation with time tracks the ice mass trajectory and provides a mean velocity estimate. Infrasound frequency is used to estimate a radius, that is in good agreement with the volume estimate from field observations. The low ($\approx 0.1 \text{ Hz}$) frequency oscillation is modeled in terms of the velocity field (wind), which the moving ice mass induces on the surrounding air, producing pressure variations at the different elements. These results show how infrasound array observations may provide quantitative information of glacier collapse and ice avalanche volume. This opens new perspectives for monitoring avalanching glaciers and providing warning for break-off events.

1 Introduction

Rapid alpine mass movements such as ice or rock avalanches, rock falls and debris flows constitute severe natural hazards. They threaten human lives and infrastructure and are expected to increase with ongoing climate change and population pressure forcing settlements into exposed terrain [Field *et al.*, 2014]. Consequently, monitoring and early warning systems, which help mitigate the threat and impact of mass movements are a key component of hazard management in mountainous regions worldwide.

Recently, glacier collapses have caught particular attention of scientists and stakeholders. The twin collapses of two Tibetan glaciers in 2017 were a sudden reminder that climate change may produce glacial hazards in new places and with unexpected dimension [Kääb *et al.*, 2018]. In Europe, costly monitoring programs have also highlighted changing glacial hazards: Glacial retreat produces new and potentially unstable ice geometries, and warming atmosphere and mountain faces change the thermal regime of already unstable ice [Raymond *et al.*, 2003; Faillietaz *et al.*, 2011b, 2015; Preiswerk *et al.*, 2016]. The latter mechanism implies that hitherto cold based ice cover frozen to steep mountain faces (“hanging glaciers”) may warm towards a temperate basal regime leading to sliding instabilities [Preiswerk *et al.*, 2016]. With most unstable ice collapses happening unnoticed, the number of well documented events is small, which complicates systematic studies of break-off activity in relation to climatic factors. Instead, successful

early warning still relies on experienced observers identifying unstable ice and subsequent monitoring.

Several studies showed that failure time of unstable ice can often be predicted because major break-off events are typically preceded by an acceleration of the ice surface [Faillettaz *et al.*, 2015]. High resolution photogrammetry and ground based interferometry (GBInSAR) [Meier *et al.*, 2016] reliably capture such acceleration, albeit at the cost of sophisticated and expensive instrument deployment, targeting only a small and pre-defined glacier region. In search of more affordable monitoring methods, researchers have turned to seismic techniques, which detect ground unrest in response to ice failure, avalanche propagation and even precursory englacial damage growth [Dalban Canassy *et al.*, 2012, 2013; Faillettaz *et al.*, 2011a; Pralong *et al.*, 2003; Faillettaz *et al.*, 2015]. Unfortunately, microseismicity near glaciers tends to mask signals related to ice break-off and to date volumes of unstable or detaching ice seracs cannot be estimated from seismic data alone.

Analogous to seismic waves, mass movements induce elastic waves in the atmosphere, which can be recorded in the infrasonic range typically taken as frequencies below 20 Hz. Snow avalanches [Naugolnykh and Bedard, 1990], rockfalls [Johnson and Ronan, 2015] and debris flows [Allstadt *et al.*, 2018; Marchetti *et al.*, 2019] have thus been studied with infrasound measurements. Although infrasound sensors are less sensitive to failure precursors, rapid detection for hazard mitigation is in principle possible. For example, infrasound detections could be used to monitor snow avalanches and debris flows in order to alert people in affected terrain and trigger road closures [Marchetti *et al.*, 2015; Schimmel *et al.*, 2018; Marchetti *et al.*, 2019].

So far, relatively little research has focused on infrasound monitoring of glacier break-off events and resulting ice avalanches. With the help of standard array methods, even weak and distant infrasound recordings can detect and locate ice break-off events [Preiswerk *et al.*, 2016]. However, it is not clear which other types of information are contained in the infrasound signature of glacier break-off events and resulting ice avalanches. In particular, volume estimates and flow velocities of ice avalanches which are key for early warning or rapid response measures have yet to be extracted from infrasound recordings of glacier break-off events.

In this study we present an infrasound analysis of a break-off from the hanging glacier at Mount Eiger, Switzerland. We show that the infrasound signature is surprisingly broad-

band containing low-frequency (0.1 Hz) pressure oscillations in addition to signals around 3 Hz, which are of the kind that has been used in previous mass movement studies. We model the low-frequency signals as pressure variations, induced by the flow of air around the moving avalanche mass. The combination of the various signal components provides good constraints on ice avalanche location, trajectory, velocity and volume.

2 Hanging Glacier on Mount Eiger, Switzerland

The hanging glacier is located at an elevation of around 3400 m above sea level on the west face of Mount Eiger in the Swiss Alps. The glacier is partly frozen to its bedrock with the presence of temperate zones [Margreth *et al.*, 2017; Faillettaz *et al.*, 2015]. Located above steep slopes, the glacier produces periodic break-off events in form of ice serac collapses from the 200 m wide and 30 m thick front, leading to ice avalanches that are typically $<10,000 \text{ m}^3$ [Margreth *et al.*, 2017]. The collapses are driven by gravity and occur upon significant englacial damage growth at a point when the ice can no longer sustain its weight [Faillettaz *et al.*, 2015]. Glacier front stability is controlled mostly by an average ice velocity at the glacier front of 7 m/y producing a yearly ice flux of 40,000 m^3 through the frontal flux gate whose area is 6,000 m^2 [Margreth *et al.*, 2017].

Given negligible surface melt, collapse events balance the ice flux, resulting in ice release events with volumes ranging between 1,000 and 100,000 m^3 . An ice collapse of 100,000 m^3 occurred on 20 August 1990 [Pralong and Funk, 2006]. If the basal thermal regime of the hanging glacier changes in response to bedrock warming and latent heat transfer, break-off failures significantly larger than 100,000 m^3 [Margreth *et al.*, 2017] may occur without any clear precursor events [Faillettaz *et al.*, 2011b].

Ice avalanches detaching from the hanging glacier front flow over 400 meters through a steep gully before entering a wider area covered with snow and ice debris produced by avalanches and previous ice collapses. Depending on this pre-existing snow cover, entrainment may enhance runout and the destructive potential of break-off events. At lower elevations, the rocky Rotstock Ridge emerges 55-110 m above its surrounding terrain, breaking and deflecting the avalanche flow southwest. This counter clockwise deflection of the flow to some extent shields the Eigergletscher train station (Figure 1). However, the train station is likely exposed to larger events that include substantial entrainment of powder snow [Margreth *et al.*, 2017].

3 Instrumentation and data

An infrasound array was deployed at an elevation of ≈ 2300 m, near the station Eigergletscher of the Jungfrau Railway (Figure 1). The main front of the hanging glacier locates ≈ 1.4 km East of and 900 m above the array.

The infrasound array was equipped with four PRS0100a pressure sensors by Item s.r.l., with a sensitivity of 25 mV/Pa in the pressure range of ± 100 Pa and frequency response between 0.02 and 100 Hz. The four sensors of the array were deployed with a triangular geometry (Figure 1), with one sensor in the center co-located with a Guralp CMG/DM24 digitizer. Maximum distance between two elements of the array was ≈ 60 m. Infrasound data provided by each array element were digitized at 24 bits and 100 Hz, GPS time stamped, recorded locally and made available through TCP/IP with a 3G modem. The pressure sensors were installed in plastic containers that were buried in the ground and covered with stones to reduce wind noise and increase the signal to noise ratio. Near the infrasound array, an interferometric radar was installed to predict break-off events via detection of unusual ice front velocities [Margreth *et al.*, 2017].

4 Serac Collapse on 29 May 2017

On May 29, 2017, a substantial serac collapse occurred from the hanging glacier at 03:45 UTC (Figure 2). The collapse was preceded by an acceleration of parts of the ice front to nearly 200 mm per day. The radar image showed that the unstable serac covered an area about 10 % larger than the equivalent 200 m^2 surface area of the 12 April 2016 break-off documented in Margreth *et al.* [2017] (Figure S1). Assuming that pervasive crevasses leading to serac separation develop 40-50 m behind the ice front [Pralong *et al.*, 2003] yields a volume estimate of $8'800\text{--}11'000\text{ m}^3$. Direct ground-based and airborne field observations estimated a volume between $20'000$ and $30'000\text{ m}^3$. Whereas the field observations cannot be reproduced, they were likely more accurate than volume estimate based on radar-derived serac area and expected crevasse location. We therefore conclude that the collapse volume was around $20'000\text{ m}^3$.

The collapsing serac fell nearly vertically for ≈ 600 m within the east-west gully and eventually turned counter-clockwise behind Rotstock Ridge before it continued moving downhill in a more or less straight line (red dashed line in Figure 1). The powder cloud reached the buildings of the Eigergletscher train station next to the infrasound an-

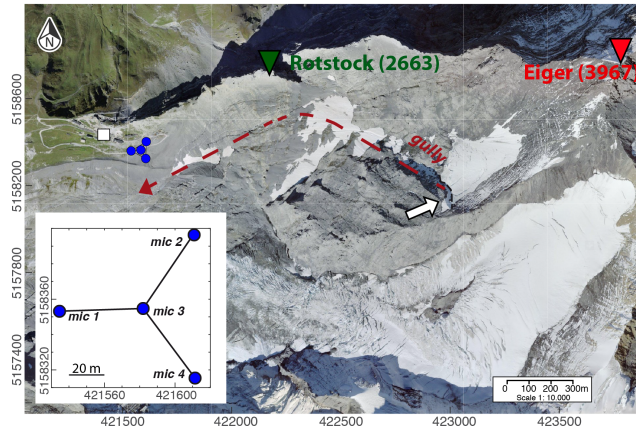


Figure 1. Location of the infrasound array (blue dots), positioned nearby the Eigergletscher train station (white square), and of the avalanching front (with arrow) of the hanging glacier on Mount Eiger. The location of Mount Eiger (reversed red triangle) and the Rotstock Ridge (reversed green triangle) peaks is marked for reference. Detached ice lamellas typically flow within a narrow gully before being deflated anti-clockwise by the Rotstock Ridge (red dashed arrow). The geometry of the four elements of the array is shown in the inset. Spot image reproduced by ©/with permission/2020 swisstopo (JD100042).

tenna and material partly covered the infrasound array. Sensor four (Figure 1, inset), in particular, was covered by snow and ice blocks.

The event was clearly recorded by the infrasound array at 03:45:10 UT, as a long-lasting (≈ 150 sec), large amplitude (> 70 Pa peak-to-peak), broadband signal (Figure 2). Higher frequency signals, peaking around 2.5–3 Hz extend to well above 10 Hz. These signals are super-imposed on a low-frequency oscillation, peaking around 0.1 Hz (Figure 2b).

The high frequency energy is most visible during the first part of the signal, until 03:45:55. The low frequency signal starts as a smooth pressure increase around 03:45:35, ≈ 25 seconds after the high frequency signal onset was recorded at the array and within a few seconds it begins to dominate the entire spectrum. The low frequency oscillations reach a first positive peak of ≈ 10 –15 Pa, within 18–23 seconds of their onset (Figure 2a). This low frequency oscillation is dispersive, showing a different frequency content at the different elements of the array. Peak frequency, measured as the inverse of the time dif-

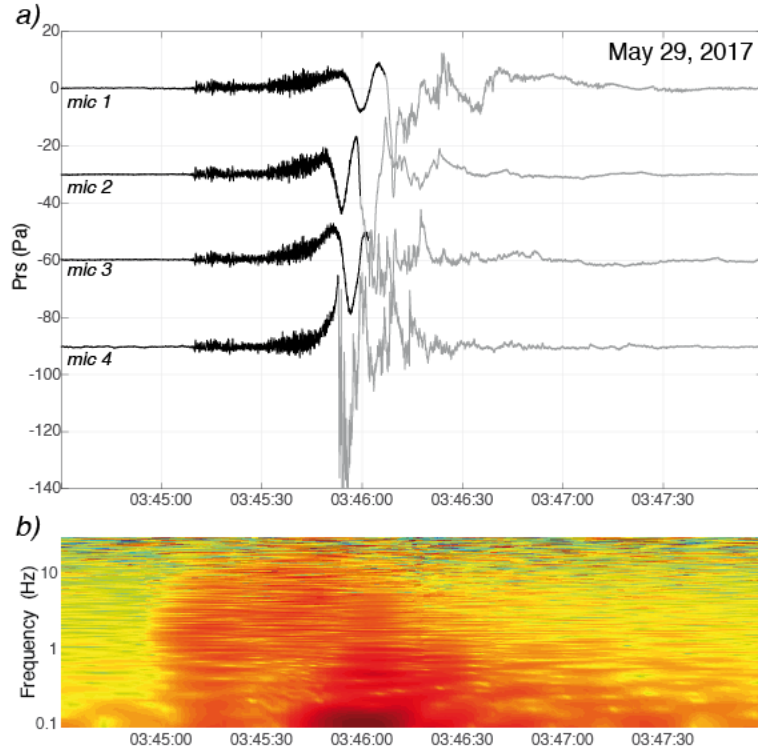


Figure 2. Infrasonic record of the collapse at the 4 elements of the array (a). The signal is colored in gray once the spurious phase is recorded. (c) Spectrogram of the signal recorded by sensor 2 showing a main peak around 0.1 Hz preceded by a higher frequency (3 Hz) phase.

ference between the two positive peaks, decreases from 0.11 Hz (9 seconds time difference) for mic 2, down to 0.085 Hz (11.6 seconds time difference) for mic 1. Moreover, the low frequency signal is marked by large time delays at the different array elements (≈ 6 seconds between mic1 and mic2 and ≈ 2.5 seconds between mic2 and mic3), with the signal first recorded at sensor 2. Considering the small aperture (≈ 85 m) of the array, these delays are consistent with a propagation velocity of a few tens of m/s, well below the propagation velocity of sound.

The waveforms show a third spurious phase (gray in Figure 2). The timing of this phase varies across the array. It is first recorded at 03:45:52 UT, before the first positive peak of the low frequency oscillation was reached, at sensor 4, and eventually, 15 seconds afterwards at 03:46:07 UT, at sensor 1. We attribute this spurious phase to avalanche debris depositing on the sensors.

5 Array Analysis of High-Frequency (3 Hz) Signals

In order to interpret the initial, high-frequency (3 Hz) infrasonic signal generated as the ice avalanche approaches the antenna, we perform coherence analysis of infrasound data recorded at the 4 array elements (Figure 3a). We apply cross-correlation analysis in discrete time windows of 5 second with 4 second overlap to 1-10 Hz band-pass filtered infrasound data. Once coherent signals are observed throughout the array, we evaluate time delays among the array elements following *Ulivieri et al.* [2011]. This gives propagation back-azimuth (Figure 3b) of the infrasound ray and allows calculation of the stacked signal along the beam (Figure 3c) as the sum of broadband (0.1-25 Hz) infrasound data recorded at the 4 array elements and shifted according to calculated propagation back-azimuth. In this way, we strongly reduce the noise and enhance the waveform characteristics. Although the stacked waveform is obtained from the broadband infrasound record, spectral analysis of stacked waveforms clearly points out a narrow frequency component peaking between 2.5 and 3 Hz (Figure 3d).

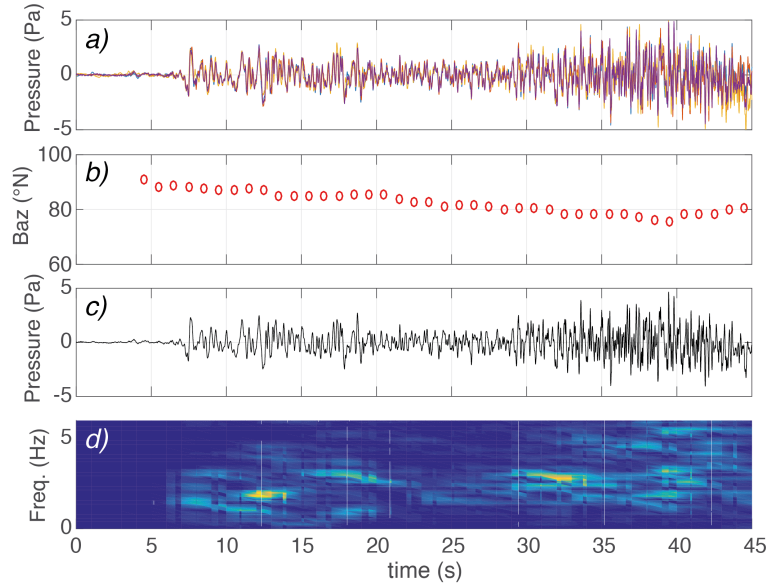


Figure 3. Amplitude (Pa at the array) of the recorded signal band-pass filtered between .1 and 25 Hz, a). Back azimuth (b) of infrasound detections. Stacked waveform along the beam (c) and corresponding PSD (d). Timing is expressed as seconds after 3:45 UTC.

Back-azimuth Baz identifies the direction of infrasound propagation and in our case defines a vector pointing from the infrasound antenna towards the moving avalanche front.

Back-azimuth is marked by a constant decrease from 90 degrees north to 75 degrees north, before the trend changes and a slight increase up to 82 degrees north is observed (Figure 3b). Considering the topography between the glacier front and the array, the observed variation of the back-azimuth is consistent with the ice mass flowing downhill within the gully to eventually turn anti-clockwise behind the Rotstock Ridge (Figure 1).

The temporal changes of back-azimuth can be used to obtain an estimate of the downhill velocity of the ice/snow mass. We assume the first detection, pointing at 90 degrees North, to be consistent with the rupture time at the front of the glacier. We assume the detection with the minimum back-azimuth of 75 degrees north, that is reached 35 seconds after the onset, to reflect the timing when the collapsing ice mass hits the Rotstock Ridge, where the direction of the gully changes from North-Westward (≈ 290 degrees N) South-Westward (≈ 235 degrees N). With this assumption, the avalanche travels a distance of ≈ 1 km between the front and the deflection point (Figure 1) in ca. 35 seconds. This corresponds to a mean velocity of ≈ 28 m/s. During this phase, recorded infrasound is characterized mostly by the high frequency component and by a smooth increase of pressure at all the sensors before the ice mass reaches the array. Our analysis thus confirms that the recorded high frequency signal, that is highly coherent across the four array elements and tracked clearly with a variable back-azimuth, is produced by the collapsed mass rapidly moving downhill.

In order to interpret the high-frequency (3 Hz) initial infrasonic signal generated as the ice avalanche approaches the antenna we approximate the avalanche volume as a moving sphere [Naugolnykh and Bedard, 1990]. Its kinetic energy is partially transferred into infrasonic wave energy as the avalanche motion perturbs atmosphere pressure. The dominant frequency of the sound wave scales with the inverse of the sphere size: [Naugolnykh and Bedard, 1990]:

$$f = c/\pi D, \quad (1)$$

where c is the velocity of sound in the atmosphere while D is the diameter of the sphere. For the 29 May 2017 collapse with a dominant infrasonic frequency of 2.5-3 Hz (Figure 3 d) and an assumed sound propagation velocity of 330 m/s, eq 1 predicts a moving sphere diameter D of ≈ 35 -42 m corresponding to a sphere volume between 22,000

and 38,000 m^3 . This result is in good agreement with the value of 20,000 m^3 estimated from the radar images and direct field observation described above.

6 Modeling the Low Frequency (0.1 Hz) Oscillation

Lack of coherence inhibits application of array techniques to the signal below 1 Hz (Figure 2 b). We propose that the low frequency (0.1 Hz) pressure oscillations are a manifestation of air streaming around the moving avalanche mass. Approximating the avalanche mass again as a rigid sphere, the behavior of the fluid is controlled by the Reynolds number (\Re), defined as:

$$\Re = Dv\rho/\mu, \quad (2)$$

where D is the diameter of the sphere, estimated above from the dominant > 1 Hz frequency to be ≈ 35 -42 m, v is its velocity, inferred to be ≈ 20 -40 m/s, and ρ and μ are the density and viscosity of air, that we assume here as 1.3 kg/m^3 and 1.7×10^{-5} Pa·s for external temperature of 0 degree C. The corresponding \Re is on the order of 10^7 , thus satisfying the assumptions for an ideal fluid ($\mu \rightarrow 0$, $\Re \rightarrow \infty$).

The problem can be described as an inviscid flow, with no boundary layer and no viscous wake downstream the sphere. In this case, the air flow around the sphere is a potential flow, where the velocity field (\mathbf{v}) is a laminar field with no vorticity and is fully described analytically by its radial (v_r) and tangential (v_θ) components [*Landau and Lifshitz*, 1959]:

$$v_r = v\left(\frac{R_S^3}{r^3}\right) \cos \theta \quad (3)$$

$$v_\theta = v\left(\frac{R_S^3}{r^3}\right) \sin \theta \quad (4)$$

where v is the velocity of the sphere, R_S is the sphere radius, r is the radial coordinate, with $r=0$ at the barycenter of the sphere, and θ represents the angular coordinate, for which $\theta=0$ in the direction of the motion of the sphere. Both equations are defined only when $r>R_S$. Both radial (eq. 3) and tangential (eq. 4) velocity components $\rightarrow 0$ with increasing distance (r) from the sphere.

According to equations (3 and 4), air molecules located along the trajectory of the sphere ($\theta=0$) have only a radial velocity component, that is positive in front of the sphere (i.e. air is pushed ahead by the sphere), while it is negative behind (i.e. air is pulled by the moving sphere). For all other positions, the air velocity field is characterized by both radial and tangential components, resulting in air flow streamlined around the sphere (Figure 4).

For each array element and following equations 3 and 4, we calculate the velocity field of air resulting from the avalanche motion (Figure 4a, b). We assumed a sphere of radius (R_S) of 20 m, in agreement with the diameter D of ≈ 35 -42 m estimated from the frequency of recorded infrasound (eq 1). The sphere moves with a velocity (v) of 28 m/s and along the collapse trajectory shown by the red dashed arrow in Figure 1 and calculated from temporal back-azimuth variations (Figure 2 c).

The velocity field \mathbf{v} (Figure 4a, b), given by equations 3 and 4, is characterized by a non-zero gradient ($\nabla \mathbf{v} \neq 0$), which means that the velocity is not constant around the sphere. Therefore, considering a unit volume V , identified by the closed surface S , at a given position nearby the sphere, influx air velocity will differ from efflux air velocity, thus resulting in $\Phi_S(\mathbf{v}) \neq 0$. This will produce, within the unit volume and in a unit time, a net air flux resulting in a change in the number (n) of air moles and thus, according to the ideal gas equation, in a change of pressure (P):

$$P = \frac{nRT}{V} \quad (5)$$

where V is the gas volume, R is ideal gas constant and T is the absolute temperature, that are all assumed as constant. The flux of the velocity field ($\Phi_S(\mathbf{v})$) is thus proportional to the net air flux and, hence, to the pressure. A quantity, which is proportional to the expected pressure P at each array element is therefore obtained from the flux of the calculated velocity field ($\Phi_S(\mathbf{v})$) via the volumetric integral of $\nabla \cdot \mathbf{v}$ and by applying the divergence theorem:

$$\Phi(\mathbf{v}) = \int_V \nabla \cdot \mathbf{v} dV \quad (6)$$

Figure 4c shows the comparison of raw infrasound data and modeling results. Amplitudes are normalized as the velocity flux ($\Phi_S(\mathbf{v})$) has been calculated with equation

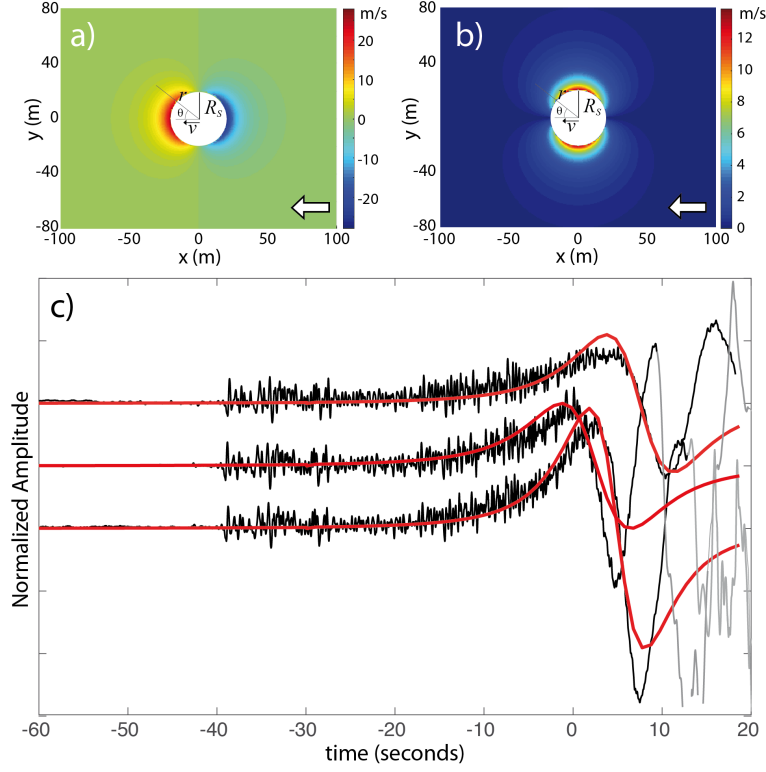


Figure 4. Radial v_r (a) and tangential v_θ (b) components of the inviscid flow induced by the moving sphere in surrounding air. The white arrow shows the sphere movement direction. Comparison (c) between the recorded infrasound pressure (black) and the modeled pressure at the array (red). Recorded waveforms are colored in gray after the spurious signal is recorded. Waveforms are normalized and aligned in time, according to the amplitude and timing of the positive peak of the second element of the array (mic2). Comparison is limited to the first 3 elements of the array where at least the first positive peak of the low frequency oscillation is fully recorded.

6 only on the plane passing through the barycenter of the sphere, whereas 3D contributions should be considered. Moreover, the relationship between $\Phi_S(\mathbf{v})$ and the air quantity was not quantified in our proposed framework.

The timing of maximum amplitude of the low frequency (0.1 Hz) oscillation at different array elements coincides with the instant when the axis connecting the sphere's barycenter and the array element is at $\theta=90$ degrees with respect to the sphere's moving direction (Figure 4c). At that point the radial velocity turns negative and the tangential velocity starts to decrease (Figure 4c) leading to a decrease of the modeled velocity flux.

7 Discussion and Conclusion

The infrasound array records of this major ice collapse ($\approx 20.000 \text{ m}^3$) from the front of the hanging glacier on Mount Eiger, Switzerland, allowed to investigate the nature of infrasound energy radiation from a falling ice mass and to evaluate the potential of infrasound array analysis to monitor avalanching glaciers.

We confirmed that a glacier collapse is an efficient source of infrasound waves, that once tracked by an array allow to evaluate the trajectory of the falling ice mass, and whose peak frequency is proportional to the ice volume. Although a more careful calibration and additional data will be required, these results highlight the potential of infrasound records to remotely estimate collapse volumes and trajectories.

Presented results show also that in certain conditions a broadband signal can be recorded, being induced by the air flux induced by the moving ice mass. Modeled and real waveforms are normalized and aligned considering the positive peak at the second element of the array (Figure 4). This allows to compare the duration, the frequency content, the relative timing and the relative amplitude of the modeled and recorded waveform. The comparison is limited to the first 3 elements of the array, where the low frequency oscillation is recorded properly. Figure 4c shows a general agreement between the recorded and modeled waveforms. The modeling reproduces the dispersive nature of the wave, the timing of the positive peaks and relative amplitude ratios. The positive peak is first recorded at sensor 2 and eventually at sensor 1, that is furthest away along the trajectory. Misfits for the signal onset might be due to the wrong assumption on the dimension and velocity of the ice collapse, the trajectory as well as the assumption of the rigid sphere instead of a mass that is likely breaking into pieces along the trajectory.

The model fails to reproduce the tail of the signal. This might result from the fact that the velocity field (\mathbf{v}) described by the equations (3) and (4) derived for inviscid flows typically fails to reproduce the velocity field behind the sphere, as it was experimentally observed that vortices develop and the flow decouples from the sphere (d’Alambert paradox [Landau and Lifshitz, 1959]). Nevertheless, our simple model explains the timing, the relative amplitude and the dispersive nature of the recorded low frequency ($< 0.1 \text{ Hz}$) infrasonic wave field, and explains the broadband frequency characteristics of the recorded signal. Given the rapid decrease of the amplitude of the velocity field with dis-

tance from the source (eq. 3 and 4) such an effect is expected primarily for data recorded near the moving source.

Ahead of confirming and validating the array processing results, the presented modeling could be used to investigate the evolution of future collapses at the hanging glacier on Mount Eiger and to understand similar signals recorded elsewhere.

Given the short computing time of infrasound array processing, and its efficiency to identify signals related to moving sources [Marchetti *et al.*, 2015], this could be used as an additional system to provide quantitative real-time information of hanging glacier stability.

Acknowledgments

We are grateful to Jungfrau Railway for allowing and supporting the installation of the infrasound array. The salary of FW was paid by the Swiss National Science Foundation (grant PP00P2_183719). We thank Lorenz Meier (Geopraevent) and Pierre Dalban Canassy (Geotest) for volume estimates of the unstable ice serac. Infrasound array data of the collapse are freely available at the OSF Open Science Framework repository (<https://osf.io/ynjm2/>).

References

- Allstadt, K.E., Matoza, R.S., Lockhart, A.B., Moran, S.C., Caplan-Auerbach, J., Haney, M.M., Thelen, W.A. and Malone, S.D. (2018). Seismic and acoustic signatures of surficial mass movements at volcanoes. *Journal of Volcanology and Geothermal Research*, 364, 76-106.
- Barfucci, G., and Ripepe, M. (2018). Dome collapse interaction with the atmosphere. *Geophys. Res. Lett.*, 45, 8923-8930, doi:10.1029/2018GL078243.
- Cramer, O. (1993). The variation of the specific heat ratio and the speed of sound in air with temperature, pressure, humidity, and CO_2 concentration. *J. Acoust. Soc. Am.* 93, 2510, doi:10.1121/1.405827.
- Dalban Canassy, P., Faillettaz, J., Walter, F., and Huss, M. (2012). Seismic activity and surface motion of a steep temperate glacier: A study on Triftgletscher, Switzerland. *J. Glaciol.* 58 (209), 513-528, doi:10.3189/2012JoG11J104.

- Dalban Canassy, P., Walter, F., Husen, S., Maurer, H., Faillettaz, J., and Farinotti, D. (2013). Investigating the dynamics of an alpine glacier using probabilistic ice-quake locations. *J. Geophys. Res. Earth Surf.* 118, 20032018, doi:10.1002/jgrf20097.
- Faillettaz, J., Funk, M., and Vincent, C. (2015). Avalanching glacier instabilities: Review on processes and early warning perspectives. *Rev. Geophys.* 53, 203-224, doi:10.1002/2014RG000466.
- Faillettaz, J., Funk, M., Sornette, D. (2011). Icequakes coupled with surface displacements for predicting glacier break-off. *J. Glaciol.* 57 (203), 453-460, doi:10.3189/002214311796905668.
- Faillettaz, J., Sornette, D., Funk, M. (2011). Numerical modeling of a gravity-driven instability of a cold hanging glacier: reanalysis of the 1895 break-off of Aletschgletscher, Switzerland. *J. Glaciol.* 57 (205), 817-831, doi:10.3189/002214311798043852.
- Field, C.B. and others (2014). Technical summary. In: ClimateChange 2014: Impacts, Adaptation, and Vulnerability. Part A: Global and Sectoral Aspects. Contribution of WorkingGroup II to the Fifth Assessment Report of the Intergovernmental Panel on Climate Change. *Cambridge University Press*, Cambridge, United Kingdom and New York, NY, USA, pp. 35-94.
- Flotron, A. (1977). Movement studies on hanging glaciers in relation with an ice avalanche. *J. Glaciol.* 19 (81), 671-672.
- Johnson, J. B., and Ronan, T. J. (2015). Infrasound from volcanic rockfalls. *J. Geoph. Res. Solid Earth* 120, 8223-8239, doi:10.1002/2015JB012436.
- Kääb, A., Leinss, S., Gilbert, A., Bühler, Y., Gascoin, S., Evans, S.G., Bartelt, P., Berthier, E., Brun, F., Chao, W.-A., Farinotti, D., Gimbert, F., Wanqin, G., Huggel, C., Kargel, J.S., Leonard, G.J., Tian, L., Treichler, D. and Yao, T. (2018). Massive collapse of two glaciers in western Tibet in 2016 after surge-like instability. *Nature Geoscience* 11(2), 114-120.
- Landau, L. D., and Lifshitz, E. M. (1959). Fluid Mechanics. *Pergamon Press*.
- Marchetti, E., Ripepe, M., Ulivieri, G., and Kogelnig, A. (2015). Infrasound array criteria for automatic detection and front velocity estimation of snow avalanches: towards a real-time early-warning system. *Nat. Hazards Earth. Syst. Sci.* 15, 2545-2555, doi:10.5194/nhess-15-2545-2015.

- Marchetti, E., Walter, F., Barfucci, G., Genco, R., Wenner, M., Ripepe, M.,
McArdell, B., and Price, C. (2019). Infrasound array analysis of debris flow ac-
tivity and implication for early warning. *J. Geoph. Res.: Earth Surface* 124,
doi:10.1029/2018JF004785.
- Marchetti, E., A. van Herwijnen, M. Christen, M. C. Silengo, and G. Barfucci2
(2020). Seismo-acoustic energy partitioning of a powder snow avalanche. *Earth
Surf. Dynam* 8, 399–411, <https://doi.org/10.5194/esurf-8-399-2020>.
- Margreth, S., Funk, M., Tobler, D., Dalban, P., Meier, L., and Lauper,
J. (2017). Analysis of the hazard caused by ice avalanches from the
hanging glacier on the Eiger west face. *Cold Reg. Sc. Tech.* 144, 63-72,
doi:10.1016/j.coldregions.2017.05.012.
- Meier, L., Jacquemart, M., Blattmann, B., Wyssen, S., Arnold, B., and Funk, M.
(2016). Radar-based warning and alarm systems for alpine mass movements. In:
Proceedings of INTRAPRAEVENT 2016, 30 May-2 June, Lucerne, Switzerland,
pp. 960-968.
- Naugolnykh, K., and Bedard, A. (1990). Model of the avalanche infrasound radia-
tion. Proceeding of International Snow Science Workshop, Jackson, WY, 19-24
September 2004, 871-872.
- Pralong, A., Funk, M. and Lüthi, M. P. (2003). A description of crevasse formation
using continuum damage mechanics. *Annals of Glaciology* 37, 77-82.
- Pralong, A., and Funk, M. (2006). On the instability of avalanching glaciers. *J.
Glaciol.* 52 (176), 31-48, doi:10.3189/172756506781828980.
- Preiswerk, L.E., Walter, F., Anandakrishnan, S., Barfucci, G., Beutel, J., Burkett,
P.G., Dalban Canassy, P., Funk, M., Limpach, P., Marchetti, E., Meier, L., Neyer,
F. (2016). Monitoring unstable parts in the ice-covered Weissmies northwest face.
13th Congress Interpraevent 2016.
- Raymond, M., Wegmann, M. and Funk, M. (2016). Inventar gefährlicher Gletscher.
VAW/ETH Report, 182.
- Schimmel, A., Hübl, J., McArdell, B.W. and Walter, F. (2018). Automatic identi-
fication of alpine mass movements by a combination of seismic and infrasound
sensors. *Sensors* 18 (5), 1658.
- Olivieri, G., Marchetti, E., Ripepe, M., Chiambretti, I., De Rosa, G., and
Segor, V. (2011). Monitoring snow avalanches in Northwestern Ital-

420 ian Alps using an infrasound array. *Cold Reg. Sci. Tech.* 69, 177–183,
421 doi:10.1916/j.coldregions.2011.09.006.